ORIGINAL PAPER

Submitted: 16.11.2021
Accepted: 25.03.2022
Early publication date: 20.09.2022

Endokrynologia Polska
DOI: 10.5603/EP.a2022.0072
ISSN 0423–104X, e-ISSN 2299–8306
Volume/Tom 73; Number/Numer 5/2022

The KLF4–p62 axis prevents vascular endothelial cell injury via the mTOR/S6K pathway and autophagy in diabetic kidney disease

Xinxing Wang[1]*, Wei Su[2]*, Mingze Ma[3], Lichao Zhu[4], Ruxin Gao[1], Chuan Qin[1], Shuai Shao[1], Dexuan Gao[5], Junlin Gao[2], Zhenhai Zhang[6]

[1]Department of Hepatobiliary Surgery, Shandong Provincial Hospital Affiliated to Shandong First Medical University, Jinan, Shandong, China
[2]Liver Gall Bladder and Pancreatic Surgery Ward, Qinghai Red Cross Hospital, Xining, Qinghai, China
[3]Department of Infectious Diseases, Shandong Provincial Hospital Affiliated to Shandong First Medical University, Jinan, Shandong, China
[4]Department of Paediatric Surgery, Shandong Provincial Hospital Affiliated to Shandong First Medical University, Jinan, Shandong, China
[5]Department of Urology, Shandong Provincial Hospital Affiliated to Shandong First Medical University, Jinan, Shandong, China
[6]Department of Hepatobiliary Surgery, Shandong Provincial Hospital, Shandong University, Jinan, Shandong, China
**These authors have contributed equally to this work and share first authorship.*

Abstract

Introduction: Diabetic kidney disease (DKD) is a complication of systemic diabetic microangiopathy, which has a high risk of developing into end-stage renal disease and death. This study explored the mechanism underlying autophagy in DKD vascular endothelial cell injury.
Material and methods: DKD and vascular endothelial cell injury models were established using Sprague Dawley rats and human umbilical vein endothelial cells (HUVECs). HUVECs overexpressing Kruppel-like factor 4 (KLF4) were constructed by transient transfection of plasmids. Biochemical determination of urinary protein and blood urea nitrogen (BUN), superoxide dismutase (SOD), and creatinine (Scr) levels was performed. Renal pathology was observed by periodic acid–Schiff (PAS) staining. Cell Counting Kit-8 (CCK8), terminal deoxynucleotidyl transferase dUTP nick end labelling (TUNEL), and immunocytochemistry (ICC) were used to analyse the growth and apoptosis of HUVECs. Microtubule-associated protein light chain 3 (LC3) expression was observed by immunofluorescence (IF). The reactive oxygen species (ROS) levels were measured using flow cytometry. Monocyte chemoattractant protein-1 (MCP-1), KLF4, and tumour necrosis factor alpha (TNF-α) levels were detected using enzyme-linked immunosorbent assay (ELISA). The expression of KLF4, p62 protein, and LC3 was analysed using reverse transcription quantitative real-time polymerase chain reaction (RT-qPCR). S6 kinase (S6K), p70 ribosomal S6 kinase (p-S6K), Beclin1, ATG5, LC3, p62, Caspase-3, mammalian target of rapamycine (mTOR), and phsophorylated mTOR (p-mTOR) expressions were detected by western blotting.
Results: PAS-positive substances (polysaccharide and glycogen) and S6K protein levels increased, and LC3 protein expression decreased in DKD rats. The levels of urinary protein, BUN, and Scr increased, and KLF4 decreased in DKD rats. High glucose (HG) levels decreased the proliferation and increased the apoptosis rate of HUVECs. The expression of ROS, TNF-α, MCP-1, and p62 increased, while the expression of SOD, KLF4, Beclin1, ATG5, and LC3 decreased in HG-induced HUVECs. KLF4 overexpression significantly increased Beclin1, ATG5, and LC3 protein expression and decreased p62 protein expression compared to the oe-NC group in HG-induced HUVECs. KLF4 overexpression inhibits the expression of Caspase-3, p-mTOR, and p-S6K in HG-induced HUVECs.
Conclusions: KLF4–p62 axis improved vascular endothelial cell injury by regulating inflammation and the mTOR/S6K pathway in DKD.
(Endokrynol Pol 2022; 73 (5): 837–845)

Key words: *Kruppel-like factor 4; human umbilical vein endothelial cells; diabetic kidney disease; mTOR/S6K pathway; autophagy*

Introduction

Worldwide, diabetic kidney disease (DKD) is the leading cause of end-stage renal disease [1]. DKD is a devastating complication of diabetes mellitus and is diagnosed based on microalbuminuria [2]. Leakage of proteins, such as albumin, through glomerular capillaries can result in the presence of albumin in the urine, which is a hallmark of kidney disease and can reflect a loss of vascular integrity in the microvascular bed, as described elsewhere [3]. DKD is also a serious microvascular complication of diabetes [4]. In addition, microvascular damage associated with hyperglycaemia leads to a vicious cycle of damaged capillaries, inflammation,

Junlin Gao, Liver Gall Bladder and Pancreatic Surgery Ward, Qinghai Red Cross Hospital, Xining, Qinghai, China; e-mail: qhhszyyybw@163.com
Zhenhai Zhang, Department of Hepatobiliary Surgery, Shandong Provincial Hospital, Shandong University, Jinan, Shandong, China; e-mail: zhangzhenhai@sdfmu.edu.cn

extracellular matrix deposition, fibrosis, and nephron loss [5]. High glucose (HG)-induced vascular endothelial cell injury is a key initiating factor for diabetic vascular complications. Therefore, studying its mechanism and corresponding protective measures has important theoretical significance and practical application value in the treatment of diabetic vascular complications.

Kruppel-like transcription factor 4 (KLF4) affects the expression of genes involved in the pathogenesis of DKD and decreases in animal models and humans with proteinuria [6]. A clinical study also found that KLF4 mRNA expression in the type 2 diabetic group was 1.60 times lower than that in the control group, and KLF4 mRNA expression in DKD was 2.92 times lower than that in the type 2 diabetic group [7]. KLF4 can also reduce transforming growth factor beta 1 (TGF-β1)-induced inflammation and fibrosis in human proximal renal tubular cells [8]. These studies have shown that KLF4 has renal protective effects in DKD, which are related to autophagy activation and inflammation and may be involved in mammalian target of rapamycine (mTOR) autophagy-related signalling pathways.

The p62/sequestosome-1 is an important selective autophagy adaptor protein, which contains a ubiquitin-related domain, Kelch-like epchloropropane-related protein field, microtubule-associated protein light chain 3 (LC3) domain, tumour necrosis factor receptor-related factor domain, Phox and Bem1p structure domain, and ZZ type zinc finger functional domains [9]. Preliminary functional assessment showed that autophagy was reduced in induced pluripotent stem cell-derived retinal pigment epithelial cells from patients with type 2 diabetes through the accumulation of ubiquitin-binding protein p62 [10]. KLF4 plays a role in promoting survival autophagy by binding to the promoter region and increasing the expression of sequentosome-1, which encodes the ubiquitin-binding adaptor protein p62 [11]. Elevated p62 levels are generally considered a marker for the inhibition of autophagy activity [11]. p62–LC3 is one of the pathways involved in autophagy-lysosomal systemic degradation, and p62 can inhibit autophagy by directly activating the mTORC1 complex [11, 12]. Autophagy is a protein and organelle degradation pathway that is dependent on lysosomal enzyme digestion, which is of great physiological significance for maintaining cell homeostasis [13]. Studying the role of autophagy in the injury of vascular endothelial cells induced by HG levels has important implications for the regulation of autophagy of vascular endothelial cells to prevent and treat diabetic vascular complications. Therefore, we hypothesized that KLF4 may regulate p62 expression and play a pro-survival autophagy role to protect DKD vascular endothelial cell damage. This study aimed to explore the mechanism of KLF4-p62 axis and autophagy in DKD to provide a theoretical basis for the treatment of DKD.

Material and methods

HUVEC culture and HG-induced HUVEC model construction

Primary HUVECs were cultured in Dulbecco's Modified Eagle Medium (DMEM) containing 10% fetal bovine serum (FBS) + 1% double antibody at 37°C, 5% CO_2, and saturated humidity. HUVECs were cultured in DMEM (5.5 mM glucose) for 12 h and then treated with 40 mM glucose (final concentration) for 24 h as a model group [14–16]. The control group was cultured in DMEM (5.5 mM glucose).

Construction of HUVECs overexpressing KLF4

Logarithmically growing HUVECs were divided into an oe-NC group (cells transfected with no-load plasmid only, oe-NC) and an oe-KLF4 group (cells transfected with 2.5 μg/mL plasmid overexpressing KAT2A, oe-KLF4). The specific steps were as follows: KLF4 overexpression plasmid and no-load plasmid were removed and defrosted on ice. Serum-free DMEM medium (95 μL) was added to two centrifuge tubes, following which 2.5 μg KLF4 overexpression plasmid (Honorgene, Changsha, China) and 5 μL Lipofectamine 2000 (11668019, Invitrogen) were added. The same procedure was performed for the oe-NC group. The 2 tubes were incubated for 5 min and mixed until a liposome complex was formed. Finally, the mixture was added evenly to the wells for transfection and mixing. After 6-h culture in a 37°C incubator, fresh complete culture medium was added.

Construction of the DKD rat model

The study protocol was approved by the Committee of Animal Care and Use of Shandong Provincial Hospital Affiliated to Shandong First Medical University (NO.2018-550) and conducted in accordance with the Declaration of Helsinki.

Twenty SPF male SD rats weighing 220–250 g were purchased from Hunan Slyke Jingda Animal Laboratory Company. Animals were randomly divided into a control and a DKD group (n = 10/group). The control group was fed normal water and diet, and the DKD group was fed a high-fat diet (HFD). After 4 weeks of HFD treatment, the DKD group was intraperitoneally injected with 50 mg/kg streptozotocin (STZ, V900890-1g, Sigma) once (fasting the night before STZ induction), and the control group was treated with an equal dose of citric acid buffer [17]. Three days after STZ induction, blood glucose was detected, and successful induction of diabetes was considered when the blood glucose value was ≥ 16.7 mm.

Periodic acid-Schiff (PAS) staining

The kidney tissue was fixed in 10% neutral buffered formalin and cut into 4-μm-thick sections. The slices of rat kidney were incubated at 60°C for 12 h and washed with distilled water after dewaxing. Then, 50 μL of periodate acid was added to quickly cover the tissue, and it was allowed to stand for 5–7 min. The slices were then washed with tap water for approximately 10 min and stained with Schiff's solution (Wellbio, Changsha, China) for 3–5 min. The slices were nucleated with haematoxylin (Wellbio, Changsha, China) for approximately 20 s (shallow staining), rinsed with distilled water, re-blued with PBS, and dried in cold air using a hair dryer. The slices were dehydrated with gradient alcohol, sealed with neutral gum, and observed under a microscope (BA410T, Motic).

TUNEL staining

The cells were fixed with 4% paraformaldehyde for 30 min and washed 3 times with PBS for 5 min each. Proteinase K working solution, TdT enzyme reaction solution, and streptavidin-TrITC labelling working solution were prepared using a TUNEL kit

(40306ES50, Shanghai Yisheng Biology), and staining treatment was carried out according to the manufacturer's instructions. The sections were stained with DAPI working solution (Wellbio, China) and washed with PBS. The sections were sealed with buffered glycerol (Wellbio, China) and observed under a fluorescence microscope (BA410T, Motic).

Immunocytochemistry (ICC)

The cells were fixed with 4% paraformaldehyde and washed with PBS. The slides were incubated with 3% H_2O_2 to inactivate endogenous enzymes at room temperature, and washed with PBS. The slides were incubated with suitably diluted primary anti-Ki67 (ab92742, 1:50, ABCAM, UK) overnight at 4°C. The slides were incubated with drops of 50–100 μL anti-rabbit IgG (H + L) antibody (SA00013-2, Proteintech, USA). DAB working solution (50–100 μL) of a prepared chromogenic agent was added to the slides. The slides were re-stained with haematoxylin and stained blue with PBS. The slides were dehydrated, sealed with neutral gum, and observed under a microscope (BA410T, Motic).

Immunofluorescence (IF)

The slices were placed in Sudan black dye solution and washed under running water. The cells were fixed with 4% paraformaldehyde. Next, 0.3% Triton was added, permeable at 37°C, and washed with PBS. The slices and cell slides were sealed with 5% BSA, incubated with suitably diluted primary anti-LC3 (14600-1-AP, 1:1000, Proteintech, USA), and rinsed with PBS overnight at 4°C. Anti-Rabbit IgG (H+L)-labelled fluorescent antibody (50–100 μL; SA00013-2, Proteintech, USA) was added, incubated at 37°C for 60–90 min, and washed 3 times with PBS for 5 min. The slices and cell slides were stained with DAPI (Wellbio, China) and rinsed with PBS. The slices and cell slides were sealed with glycerine buffer (Wellbio, China) and observed under a fluorescence microscope (BA410T, Motic).

Biochemical tests

The urine protein quantitative test kit (C035-2-1, NJIBE, China), urea nitrogen test kit (C013-2-1, NJIBE, China), creatinine determination kit (C011-2-1, NJIBE, China), and superoxide dismutase (SOD) assay kit (A001-3-2, NJIBE, China), along with a Multifunctional Enzyme Marker Analyzer (MB-530, HEALES), were used to analyse the urinary protein, BUN, Scr, and SOD using the CBB, urease, WST-1, and sarcosine oxidase methods, respectively.

Flow cytometry

The cell precipitate was collected by centrifugation, washed once with RPMI 1640 complete medium (R8758, Sigma), and centrifuged at 1500 rpm for 5 min, and the supernatant was discarded. DCFH-DA (S0033S, Beyotime Biotechnology) with serum-free medium at 1:1000. Diluted DCFH-DA was added to the cell precipitate to suspend the cells. The cells were then incubated in the dark and collected by centrifugation. The green fluorescence of ROS-FITC (excitation wavelength, Ex = 488 nm; emission wavelength, Em = 530 nm) was detected using a flow cytometer (A00-1-1102, Beckman) via the FITC channel.

ELISA

Whole blood samples were placed at room temperature for 2 h and centrifuged at 2–8°C at 1000 g for 15 min, to collect the supernatant for detection. The supernatant of cell cultures was collected for detection by centrifugation at 2–8°C and 1000 g for 15 min. The cells were washed and transferred to an appropriate centrifuge tube, and 1 × PBS (pH = 7.2–7.4) was added. After the cell membrane was destroyed by ultrasonic crushing, the cells were centrifuged at 2–8°C and 5000 g for 5 min to remove the supernatant for detection. Monocyte chemoattractant protein-1 (MCP-1) (CSB-E04655H, CUSABIO), tumour necrosis factor alpha (TNF-α) (CSB-E04740H, CUSABIO), and KLF4 (JL51834, Shanghai Jianglai Biotechnology Co., Ltd) and a Multifunctional Enzyme Marker Analyzer (MB-530, HEALES) were used to analyse MCP-1, TNF-α, and KLF4 levels in blood, cell supernatant, and cells, respectively.

CCK8

The cells were digested, counted, and inoculated at a density of 5×10^3 cells/well in a 96-well plate (0030730119, Eppendorf). CCK8 solution prepared with complete medium at a ratio of 1:9, and 10 μL/well CCK8 (NU679, Japanese counterparts), was added to each well. The absorbance value was analysed using a Multifunctional Enzyme Marker Analyzer (MB-530, HEALES) after further incubation at 37°C for 4 h.

RT-qPCR

After the experiment, kidney tissues and HUVECs were collected, and total RNA from tissues and cells was extracted using TRIzol reagent (Thermo, USA). cDNA was synthesized using a reverse transcription kit (CW2569; CWBio, China). The primer sequences were as follows: KLF4, F AAGTCCCGCCGCTCCATTACCAA, R CATCATCCCGTGTGTCCCGAAG; LC3, F GCGAGTTACCTCCCGCAG, R GTACCTCCTTACAGCGGTCG; P62, F GGTCGCGCTCACCTTTCT, R TCCTTTCTCAAGCCCCATGTT; and β-actin, F ACCCTGAAGTACCCCATCGAG, R AGCACAGCCTGGATAGCAAC. mRNA expression levels were analysed using the UltraSYBR Mixture (CW2601, CWBIO, China) and the $2^{-\Delta\Delta CT}$ method.

Western blotting

Kidney tissues and HUVECs were collected, and the protein concentration was determined by radioimmunoprecipitation analysis (RIPA), lysis buffer solution, and bicinchoninic acid (BCA) method. Proteins were separated by 12% sodium dodecyl sulphate-polyacrylamide gel electrophoresis (SDS-PAGE). The isolated proteins were transferred onto polyvinylidene fluoride (PVDF) membranes. The primary antibody was then incubated at 4°C overnight. The antibodies included anti-S6K (ab32529, 1:5000, Abcam, UK), anti-p-S6K (ab32529, 1:5000, Abcam, UK), anti-Beclin1 (11306-1-AP, 1: 5000, Proteintech, USA), anti-ATG5 (ab109490, 1:5000, Abcam, UK), anti-LC3 (14600-1-AP, 1: 1000, Proteintech, USA), anti-p62 (18420-1-AP, 1:2000, Proteintech, USA), anti-KLF4 (11880-1-AP, 1: 500, Proteintech, USA), anti-caspase 3 (19677-1-AP, 1:500, Proteintech, USA), anti-p-mTOR (ab109268, 1: 5000, Abcam, Cambridge, UK), anti-mTOR (ab32028, 1:2000, Abcam, UK), and anti-β-actin (60008-1-IG, 1:5000, Proteintech, USA). It was then combined with secondary anti-IgG antibodies (1:5000, SA00001-1; 1:6000, SA00001-2, Proteintech, USA). Visualization and imaging analyses were performed using chemiluminescence (Millipore, USA) and imaging software (GE Healthcare, Life Sciences, USA).

Data analysis and processing

SPSS 21.0 (IBM, USA) was used for statistical analysis of the data in this study. The measurement data are expressed as mean ± standard deviation. First, normality and homogeneity of variance tests were performed. The test conformed to a normal distribution, and the variance was homogeneous. The non-paired t-test was used between groups, one-way ANOVA or ANOVA of repeated measurement data was used for a multigroup comparison, and Tukey's post hoc test was carried out. $p < 0.05$ indicated that the difference was considered statistically significant.

Results

KLF4 expression was related to autophagy in DKD model rats

Pathological observation of the renal tissue revealed that PAS-positive substances (polysaccharides

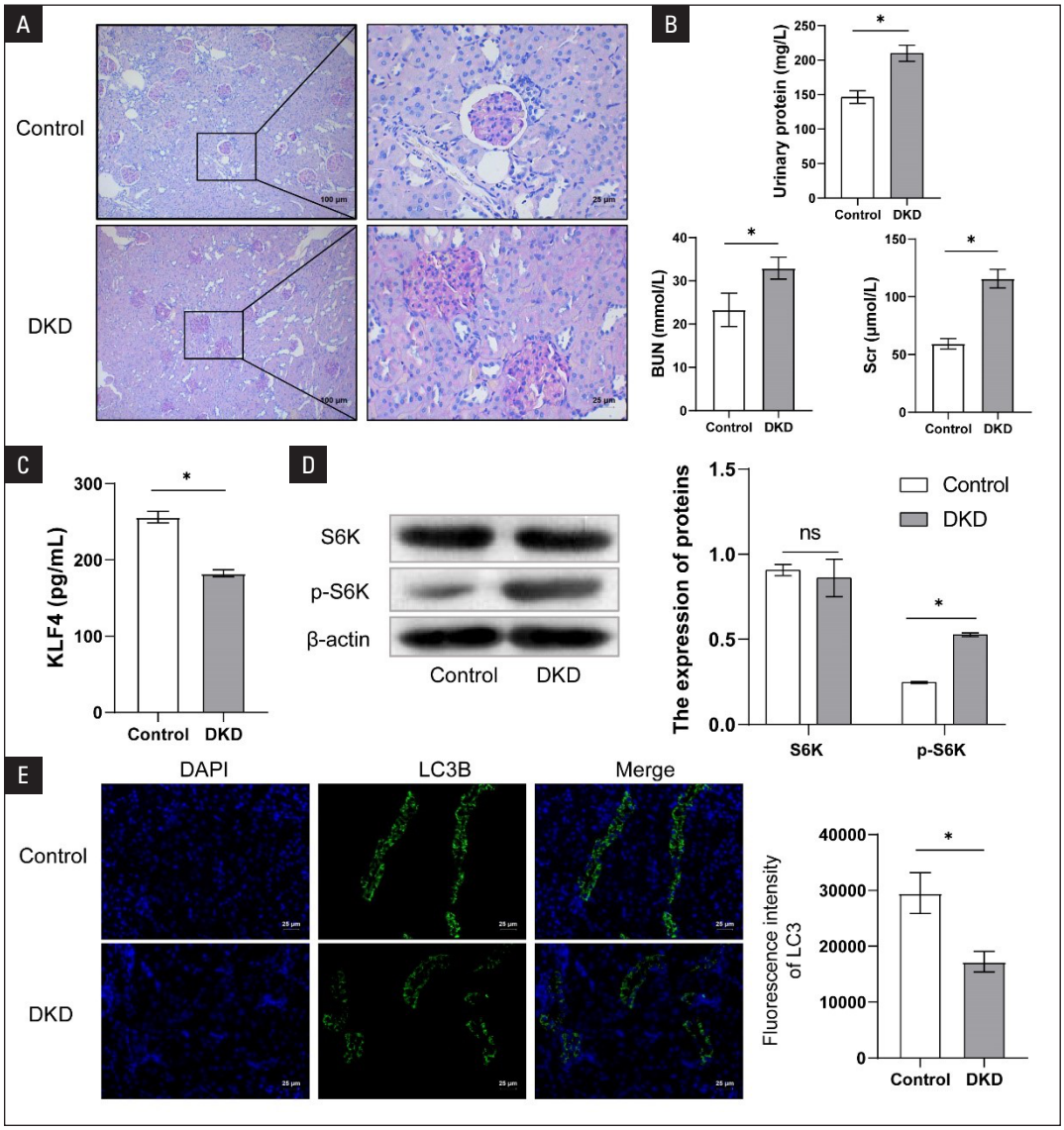

Figure 1. *Construction of a diabetic kidney disease (DKD) mouse model and pathological changes in kidney tissue.* **A.** *Periodic acid–Schiff (PAS) staining was used to observe the pathological changes in renal tissue structure (Scale bar = 100 μm; magnification 100×. Scale bar = 25 μm; magnification 400×);* **B.** *Analysis of 24-hour urinary protein, blood urea nitrogen (BUN), and creatinine (Scr) levels;* **C.** *Enzyme-linked immunosorbent assay (ELISA) analysis of Kruppel-like factor 4 (KLF4);* **D.** *Western blot analysis of the autophagy-related receptor S6 kinase (S6K) and p70 ribosomal S6 kinase (p-S6K) protein expression;* **E.** *Microtubule-associated protein light chain 3 (LC3) expression detected by immunofluorescence staining (Scale bar = 25 μm; magnification 400×). *Compared with control group, $p < 0.05$*

and glycogen) were red or purplish red with blue nuclei (Fig. 1A). Compared with those in the control group, PAS-positive substances (polysaccharide and glycogen) increased significantly in the DKD group (Fig. 1A). A routine 24-h blood analysis showed increased urinary protein, BUN, and Scr levels in the DKD group (Fig. 1B). KLF4 levels in the blood of DKD rats were decreased (Fig. 1C). Autophagy-related protein detection showed that the phosphorylation of S6K protein increased and the expression of LC3 protein decreased in the DKD group (Fig. 1D, E). These results suggested that KLF4 expression in the DKD model rats may be related to autophagy.

KLF4 expression was low in HG-induced HUVECs

We constructed a vascular endothelial cell injury model of HG-induced HUVECs, and CCK8 detection showed that the growth of HUVECs in the model group decreased (Fig. 2A). HG induced severe apoptosis of HUVECs (Fig. 2B), and HG treatment increased reactive oxygen species (ROS) levels and decreased SOD levels in HUVECs (Fig. 2C, D). An inflammatory factor analysis showed that TNF-α and MCP-1 levels were increased in HG-induced HUVECs (Fig. 2E). Compared with that in the control group, the HG-induced expression of KLF4 in HUVECs decreased significantly (Fig. 2F).

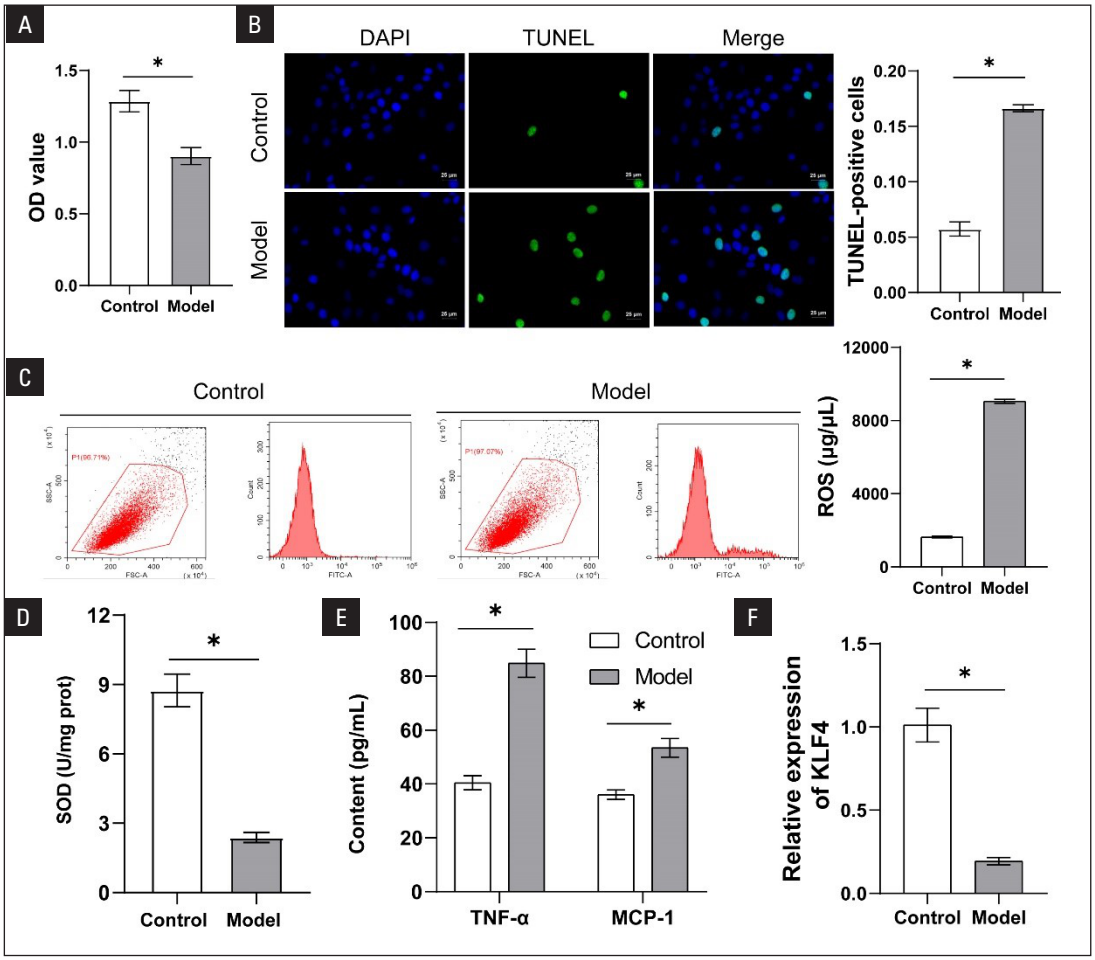

Figure 2. *High glucose induced human umbilical vein endothelial cells (HUVEC) damage and inflammation.* **A.** *Cell proliferation detected by Cell Counting Kit 8 (CCK-8);* **B.** *Apoptosis detected by terminal deoxynucleotidyl transferase dUTP nick end labeling (TUNEL) staining (Scale bar = 25 μm; magnification 400×);* **C.** *Reactive oxygen species (ROS) levels detected by flow cytometry.* **D.** *Superoxide dismutase (SOD) levels detected by the WST-1 method;* **E.** *Expression of tumour necrosis factor alpha (TNF-α) and monocyte chemoattractant protein-1 (MCP-1) detected by enzyme-linked immunosorbent assay (ELISA);* **F.** *Kruppel-like factor 4 (KLF4) expression detected by reverse transcription quantitative real-time (RT-qPCR). *Compared with control group, $p < 0.05$*

These results indicated that HG levels induced HUVEC injury and low expression of KLF4.

HG inhibited HUVEC autophagy

We detected autophagy levels induced by HG in HUVECs. The IF analysis showed that the fluorescence intensity of the LC3 protein in the model group decreased (Fig. 3A). Compared to that in the control group, expression of Beclin1, ATG5, and LC3 proteins decreased significantly, and that of p62 increased significantly in the model group (Fig. 3B). These results indicated that HG inhibited autophagy in HUVECs.

Overexpression of KLF4 regulated the expression of p62 and promoted survival autophagy

We constructed KLF4-overexpressed HUVECs and established an HG-induced cell injury model. Compared with those in the oe-NC group, KLF4 and LC3 expressions increased significantly, and the expression of p62 decreased significantly in the oe-KLF4 group (Fig. 4A). The protein expression analysis showed that Beclin1, ATG5, and LC3 expression increased significantly and p62 expression decreased significantly in the oe-KLF4 group (Fig. 4B). Overexpression of KLF4 regulated the expression of p62 and promoted HG-induced survival of HUVECs.

Overexpression of KLF4 improved HUVEC damage by inhibiting the mTOR/S6K pathway

The flow cytometry analysis showed that KLF4 overexpression decreased ROS levels in HG-induced HUVECs (Fig. 5A). KLF4 overexpression increased SOD levels in HG-treated HUVECs (Fig. 5B), decreased TNF-α and MCP-1 levels in HG-induced HUVECs

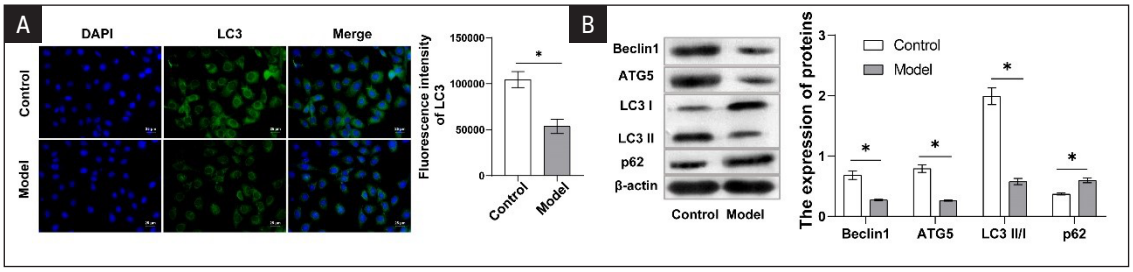

Figure 3. *High glucose inhibited the autophagy of human umbilical vein endothelial cells (HUVECs).* **A.** *Microtubule-associated protein light chain 3 (LC3) expression detected by immunofluorescence (scale bar = 25 μm; magnification 400×);* **B.** *Western blot analysis of the protein expression of Beclin1, ATG5, LC3, and p62. *Compared with control group, $p < 0.05$*

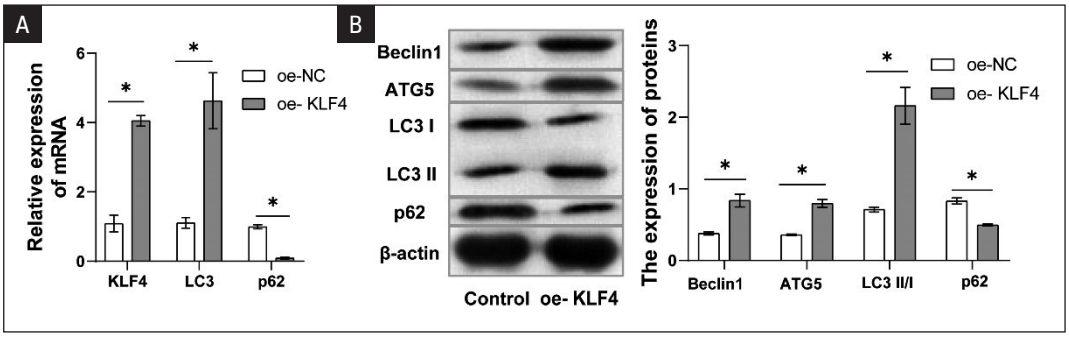

Figure 4. *Overexpression of Kruppel-like factor 4 (KLF4) regulated human umbilical vein endothelial cells (HUVECs) autophagy.* **A.** *Expression of Kruppel-like factor 4 (KLF4), microtubule-associated protein light chain 3 (LC3), and p62 detected by reverse transcription quantitative real-time (RT-qPCR);* **B.** *Protein expression of Beclin1, ATG5, LC3, and p62 detected by western blot. *Compared with oe-NC group, $p < 0.05$*

(Fig. 5C), and promoted HG-induced proliferation of HUVECs (Fig. 5D). The protein expression analysis showed that KLF4 overexpression inhibited the expressions of Caspase-3, mTOR, and S6K in HG-induced HUVECs (Fig. 5E, F). These results suggested that KLF4 overexpression protected against HUVEC injury in DKD by inhibiting the mTOR/S6K pathway.

Discussion

DKD is a major microvascular complication of diabetes [18]. The natural course of DKD includes glomerular hyperfiltration, progressive proteinuria, decreased glomerular filtration rate, and end-stage renal disease [19]. The STZ rat model, the most widely used model of type 1 diabetes, presents significant renal morphological changes similar to human DKD, including hyperglycaemia, mesangial area dilation, and proteinuria [20]. STZ-induced DKD rats showed increased urinary protein, creatinine, urea nitrogen, and renal hypertrophy index, as well as inflammatory cell infiltration and renal interstitial fibrosis [21]. Our study showed that PAS-positive substances (polysaccharides and glycogen) and S6K proteins were increased and LC3 protein was decreased in DKD rats. Moreover, the levels of urinary protein, BUN, and Scr increased, and KLF4 decreased in DKD rats. These results were consistent with previous reports, confirming that the DKD model constructed in this study could be used for further research.

Insufficient podocyte autophagy in diabetic patients and rats, accompanied by high proteinuria and podocyte loss, suggest that autophagy plays a key role in maintaining podocyte lysosomal homeostasis in diabetic patients [22]. Our study showed that, compared with that in normal rats, the renal injury of diabetic rats was aggravated, the renal autophagy level of DKD rats was inhibited, and the expression level of LC3 decreased [23]. In addition, a very low-protein diet may ameliorate advanced diabetic kidney injury, including tubulointerstitial injury, by inhibiting the mTORC1 pathway to restore autophagy [24]. The above-mentioned studies prove that we successfully constructed a DKD rat model, and autophagy is a potential target for the treatment of DKD; however, its mechanism requires further study.

Autophagy is an important mechanism for maintaining glomerular and tubule homeostasis and plays an important role in human health and disease [25]. Ablation of the proximal renal tubule autophagy-associated gene 7 leads to autophagy deficiency and more

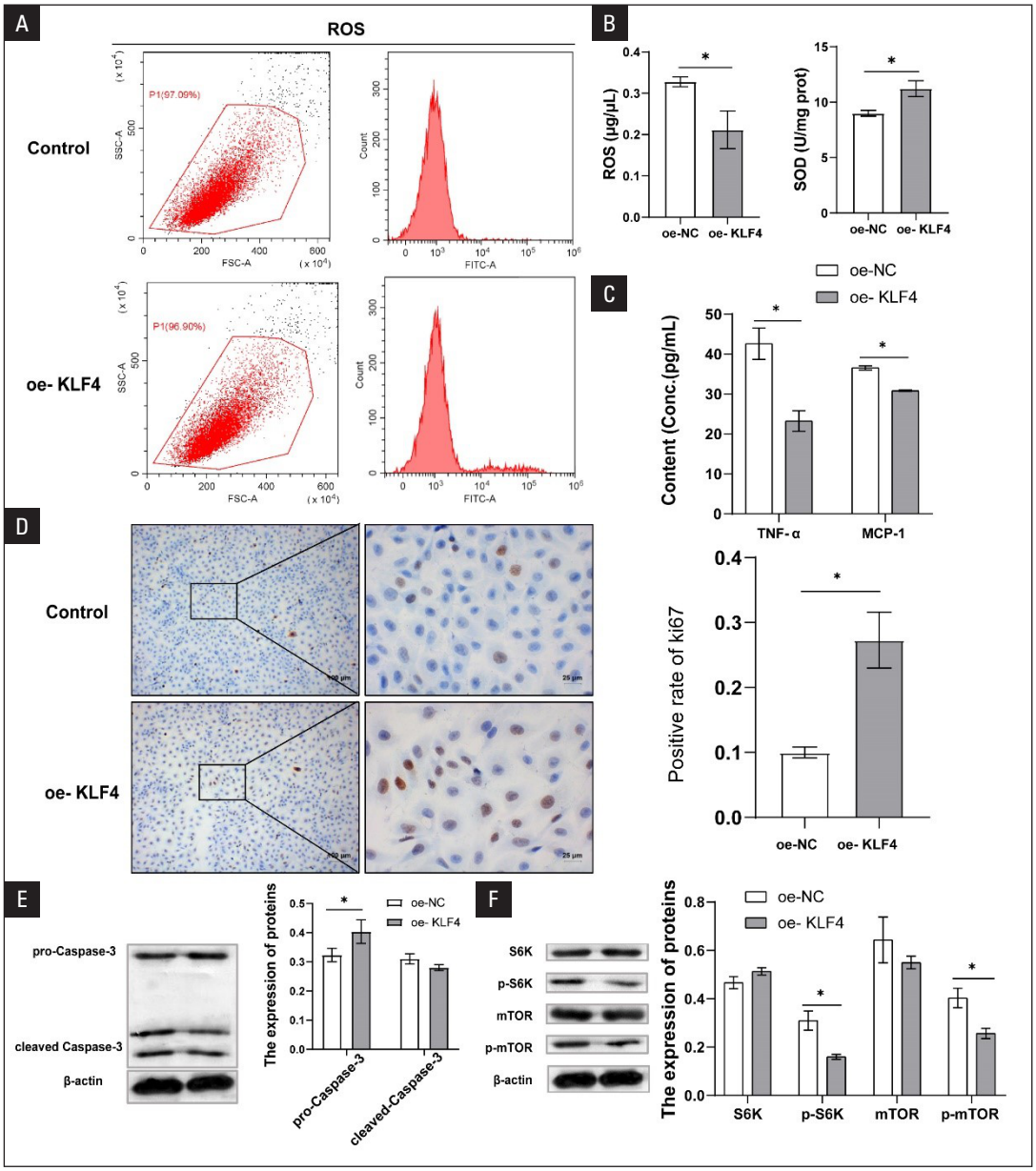

Figure 5. *Overexpression of Kruppel-like factor 4 (KLF4) improved human umbilical vein endothelial cells (HUVECs) damage by inhibiting the mammalian target of rapamycine (mTOR)/S6 kinase (S6K) pathway.* **A.** *Reactive oxygen species (ROS) levels detected by flow cytometry;* **B.** *Superoxide dismutase (SOD) levels detected by WST-1 method;* **C.** *Levels of tumour necrosis factor alpha (TNF-α) and monocyte chemoattractant protein-1 (MCP-1) were detected by enzyme-linked immunosorbent assay (ELISA);* **D.** *Immunocytochemical analysis of Ki-67 expression (Scale bar = 100 μm; magnification 100×. Scale bar = 25 μm; magnification 400×);* **EF.** *Protein expression of Caspase-3, S6K, mTOR, phsophorylated mTOR (p-mTOR), and p70 ribosomal S6 kinase (p-S6K) detected by western blot. *Compared with oe-NC group, $p < 0.05$*

severe renal hypertrophy, tubular injury, inflammation, fibrosis, and proteinuria in diabetic mice, suggesting that autophagy plays a protective role in DKD [26]. Evidence of the protective role of autophagy in kidney disease has stimulated interest in autophagy as a potential therapeutic strategy [27]. In this study, HUVECs were induced by HG to construct an in vitro model, which showed that cell proliferation decreased, the apoptosis rate increased, ROS, TNF-α, MCP-1, and p62 protein expression levels increased, and SOD, KLF4, Beclin1, ATG5, and LC3 protein expression levels decreased. Renal macrophage infiltration is the main pathological feature of DKD [28, 29]. High fructose intake during pregnancy leads to long-term changes in renal inflammation and autophagic flux in adult female offspring [30]. These studies have shown that inhibition of autophagy is related to renal inflammatory infiltration and glomerular injury, and activation of autophagy might be an effective method to treat DKD.

The enhancement of autophagy response can improve the renal dysfunction of DKD [31]. Hepatocellular growth factor-treated diabetic mice showed increased autophagic activity, such as decreased p62 accumulation and increased microtubule-associated protein LC3 II/I ratio [32]. KLF4 plays a key role in autophagy regulation and inhibition of mTOR activity, which can prevent DNA damage and cell apoptosis by activating autophagy [33]. Knockout of KLF4 attenuates YAP increase and nuclear translocation, as well as renal deterioration and interstitial fibrosis in ischaemia-reperfusion mice, whereas KLF4 overexpression leads to the opposite effect [34]. Our study also found that overexpression of KLF4 increased Beclin1, ATG5, and LC3 protein expression, decreased p62 protein expression compared to the oe-NC group, and promoted the activity of HG-induced HUVECs. Our results confirm that KLF4 may play a potential protective role through autophagy, which is consistent with the aforementioned studies.

In addition, KLF4 overexpression reduced the levels of urinary albumin, Scr, and BUN in rats with DKD and decreased mesangial matrix expansion and mesangial cell proliferation [35]. Following the in vitro overexpression of KLF4, the expression levels of the p-mTOR and p-S6K proteins decreased [35]. KLF4 regulates the reduction of autophagy in human aortic vascular smooth muscle cells induced by hyperhomocysteine through the mTOR signalling pathway [36]. Activation of KLF4 can enhance autophagy and M2 polarization of macrophages [37]. Similarly to these studies, our study also found that KLF4 overexpression inhibited the expression of Caspase-3, mTOR, and S6K proteins in HG-treated HUVECs. Therefore, our study proved that the KLF4–p62 axis regulates the survival autophagy of the m-TOR/S6K pathway to protect against DKD vascular endothelial cell damage, to provide a theoretical basis for the treatment of DKD.

Acknowledgements

This work was supported by the National Natural Science Foundation of China (No. 81870205), Chen Xiao-Ping Foundation for the Development of Science and Technology of Hubei Province (CXPJJH12000001-2020304), Foundation Research Project of Qinghai Province (2021-ZJ-719), and National Natural Science Foundation of China (No. 82000579).

Conflict of interest

The authors declare that they have no conflict of interests.

References

1. Qi C, Mao X, Zhang Z, et al. Classification and Differential Diagnosis of Diabetic Nephropathy. J Diabetes Res. 2017; 2017: 8637138, doi: 10.1155/2017/8637138, indexed in Pubmed: 28316995.
2. Papadopoulou-Marketou N, Kanaka-Gantenbein C, Marketos N, et al. Biomarkers of diabetic nephropathy: A 2017 update. Crit Rev Clin Lab Sci. 2017; 54(5): 326–342, doi: 10.1080/10408363.2017.1377682, indexed in Pubmed: 28956668.
3. Desideri S, Onions KL, Baker SL, et al. Endothelial glycocalyx restoration by growth factors in diabetic nephropathy. Biorheology. 2019; 56(2-3): 163–179, doi: 10.3233/BIR-180199, indexed in Pubmed: 31156139.
4. Nagib AM, Elsayed Matter Y, Gheith OA, et al. Diabetic Nephropathy Following Posttransplant Diabetes Mellitus. Exp Clin Transplant. 2019; 17(2): 138–146, doi: 10.6002/ect.2018.0157, indexed in Pubmed: 30945628.
5. Hesp AC, Schaub JA, Prasad PV, et al. The role of renal hypoxia in the pathogenesis of diabetic kidney disease: a promising target for newer renoprotective agents including SGLT2 inhibitors? Kidney Int. 2020; 98(3): 579–589, doi: 10.1016/j.kint.2020.02.041, indexed in Pubmed: 32739206.
6. Hayashi K, Sasamura H, Nakamura M, et al. KLF4-dependent epigenetic remodeling modulates podocyte phenotypes and attenuates proteinuria. J Clin Invest. 2014; 124(6): 2523–2537, doi: 10.1172/JCI69557, indexed in Pubmed: 24812666.
7. Coskun ZM, Ersoz M, Adas M, et al. Kruppel-Like Transcription Factor-4 Gene Expression and DNA Methylation Status in Type 2 Diabetes and Diabetic Nephropathy Patients. Arch Med Res. 2019; 50(3): 91–97, doi: 10.1016/j.arcmed.2019.05.012, indexed in Pubmed: 31495395.
8. Mreich E, Chen XM, Zaky A, et al. The role of Krüppel-like factor 4 in transforming growth factor-β-induced inflammatory and fibrotic responses in human proximal tubule cells. Clin Exp Pharmacol Physiol. 2015; 42(6): 680–686, doi: 10.1111/1440-1681.12405, indexed in Pubmed: 25882815.
9. Milan E, Perini T, Resnati M, et al. A plastic SQSTM1/p62-dependent autophagic reserve maintains proteostasis and determines proteasome inhibitor susceptibility in multiple myeloma cells. Autophagy. 2015; 11(7): 1161–1178, doi: 10.1080/15548627.2015.1052928, indexed in Pubmed: 26043024.
10. Kiamehr M, Klettner A, Richert E, et al. Compromised Barrier Function in Human Induced Pluripotent Stem-Cell-Derived Retinal Pigment Epithelial Cells from Type 2 Diabetic Patients. Int J Mol Sci. 2019; 20(15), doi: 10.3390/ijms20153773, indexed in Pubmed: 31375001.
11. Riz I, Hawley TS, Hawley RG. KLF4-SQSTM1/p62-associated prosurvival autophagy contributes to carfilzomib resistance in multiple myeloma models. Oncotarget. 2015; 6(17): 14814–14831, doi: 10.18632/oncotarget.4530, indexed in Pubmed: 26109433.
12. Mei Q, Zeng Y, Huang C, et al. Rapamycin Alleviates Hypertriglyceridemia-Related Acute Pancreatitis via Restoring Autophagy Flux and Inhibiting Endoplasmic Reticulum Stress. Inflammation. 2020; 43(4): 1510–1523, doi: 10.1007/s10753-020-01228-7, indexed in Pubmed: 32642911.
13. Levine B, Kroemer G. Biological Functions of Autophagy Genes: A Disease Perspective. Cell. 2019; 176(1-2): 11–42, doi: 10.1016/j.cell.2018.09.048, indexed in Pubmed: 30633901.
14. Zhou Y, Qi C, Li S, et al. Investigation of the Mechanism Underlying Calcium Dobesilate-Mediated Improvement of Endothelial Dysfunction and Inflammation Caused by High Glucose. Mediators Inflamm. 2019; 2019: 9893682, doi: 10.1155/2019/9893682, indexed in Pubmed: 31780874.
15. Zhou Y, Yuan J, Qi C, et al. Calcium dobesilate may alleviate diabetesinduced endothelial dysfunction and inflammation. Mol Med Rep. 2017; 16(6): 8635–8642, doi: 10.3892/mmr.2017.7740, indexed in Pubmed: 29039485.
16. Chen J, Zhang W, Xu Q, et al. Ang-(1-7) protects HUVECs from high glucose-induced injury and inflammation via inhibition of the JAK2/STAT3 pathway. Int J Mol Med. 2018; 41(5): 2865–2878, doi: 10.3892/ijmm.2018.3507, indexed in Pubmed: 29484371.
17. Liu C, Zhao S, Zhu C, et al. Ergosterol ameliorates renal inflammatory responses in mice model of diabetic nephropathy. Biomed Pharmacother. 2020; 128: 110252, doi: 10.1016/j.biopha.2020.110252, indexed in Pubmed: 32446112.
18. Lu Y, Liu D, Feng Qi, et al. Diabetic Nephropathy: Perspective on Extracellular Vesicles. Front Immunol. 2020; 11: 943, doi: 10.3389/fimmu.2020.00943, indexed in Pubmed: 32582146.
19. Alicic RZ, Rooney MT, Tuttle KR. Diabetic Kidney Disease: Challenges, Progress, and Possibilities. Clin J Am Soc Nephrol. 2017; 12(12): 2032–2045, doi: 10.2215/CJN.11491116, indexed in Pubmed: 28522654.
20. Giralt-López A, Molina-Van den Bosch M, Vergara A, et al. Revisiting Experimental Models of Diabetic Nephropathy. Int J Mol Sci. 2020; 21(10), doi: 10.3390/ijms21103587, indexed in Pubmed: 32438732.
21. Xiang E, Han B, Zhang Q, et al. Human umbilical cord-derived mesenchymal stem cells prevent the progression of early diabetic nephropathy through inhibiting inflammation and fibrosis. Stem Cell Res Ther. 2020; 11(1): 336, doi: 10.1186/s13287-020-01852-y, indexed in Pubmed: 32746936.
22. Tagawa A, Yasuda M, Kume S, et al. Impaired Podocyte Autophagy Exacerbates Proteinuria in Diabetic Nephropathy. Diabetes. 2016; 65(3): 755–767, doi: 10.2337/db15-0473, indexed in Pubmed: 26384385.
23. Jiang Y, Zhao Yu, Zhu X, et al. Effects of autophagy on macrophage adhesion and migration in diabetic nephropathy. Ren Fail. 2019;

41(1): 682–690, doi: 10.1080/0886022X.2019.1632209, indexed in Pubmed: 31352855.
24. Kitada M, Ogura Y, Suzuki T, et al. A very-low-protein diet ameliorates advanced diabetic nephropathy through autophagy induction by suppression of the mTORC1 pathway in Wistar fatty rats, an animal model of type 2 diabetes and obesity. Diabetologia. 2016; 59(6): 1307–1317, doi: 10.1007/s00125-016-3925-4, indexed in Pubmed: 27020449.
25. Ding Y, Choi ME. Autophagy in diabetic nephropathy. J Endocrinol. 2015; 224(1): R15–R30, doi: 10.1530/JOE-14-0437, indexed in Pubmed: 25349246.
26. Ma Z, Li L, Livingston MJ, et al. p53/microRNA-214/ULK1 axis impairs renal tubular autophagy in diabetic kidney disease. J Clin Invest. 2020; 130(9): 5011–5026, doi: 10.1172/JCI135536, indexed in Pubmed: 32804155.
27. Sakai S, Yamamoto T, Takabatake Y, et al. Proximal Tubule Autophagy Differs in Type 1 and 2 Diabetes. J Am Soc Nephrol. 2019; 30(6): 929–945, doi: 10.1681/ASN.2018100983, indexed in Pubmed: 31040190.
28. Hickey FB, Martin F. Role of the Immune System in Diabetic Kidney Disease. Curr Diab Rep. 2018; 18(4): 20, doi: 10.1007/s11892-018-0984-6, indexed in Pubmed: 29532281.
29. Østergaard JA, Jha JC, Sharma A, et al. Adverse renal effects of NLRP3 inflammasome inhibition by MCC950 in an interventional model of diabetic kidney disease. Clin Sci (Lond). 2022; 136(2): 167–180, doi: 10.1042/CS20210865, indexed in Pubmed: 35048962.
30. Sato S, Norikura T, Mukai Y. Maternal quercetin intake during lactation attenuates renal inflammation and modulates autophagy flux in high-fructose-diet-fed female rat offspring exposed to maternal malnutrition. Food Funct. 2019; 10(8): 5018–5031, doi: 10.1039/c9fo01134j, indexed in Pubmed: 31355385.
31. Dusabimana T, Kim SoRa, Park EJ, et al. P2Y2R contributes to the development of diabetic nephropathy by inhibiting autophagy response. Mol Metab. 2020; 42: 101089, doi: 10.1016/j.molmet.2020.101089, indexed in Pubmed: 32987187.
32. Hou Bo, Li Y, Li X, et al. HGF protected against diabetic nephropathy via autophagy-lysosome pathway in podocyte by modulating PI3K/Akt-GSK3β-TFEB axis. Cell Signal. 2020; 75: 109744, doi: 10.1016/j.cellsig.2020.109744, indexed in Pubmed: 32827692.
33. Liu C, DeRoo EP, Stecyk C, et al. Impaired autophagy in mouse embryonic fibroblasts null for Krüppel-like Factor 4 promotes DNA damage and increases apoptosis upon serum starvation. Mol Cancer. 2015; 14: 101, doi: 10.1186/s12943-015-0373-6, indexed in Pubmed: 25944097.
34. Xu D, Chen PP, Zheng PQ, et al. KLF4 initiates sustained YAP activation to promote renal fibrosis in mice after ischemia-reperfusion kidney injury. Acta Pharmacol Sin. 2021; 42(3): 436–450, doi: 10.1038/s41401-020-0463-x, indexed in Pubmed: 32647339.
35. Gong J, Zhan H, Li Y, et al. Krüppellike factor 4 ameliorates diabetic kidney disease by activating autophagy via the mTOR pathway. Mol Med Rep. 2019; 20(4): 3240–3248, doi: 10.3892/mmr.2019.10585, indexed in Pubmed: 31432191.
36. Ni T, Gao F, Zhang J, et al. Impaired autophagy mediates hyperhomocysteinemia-induced HA-VSMC phenotypic switching. J Mol Histol. 2019; 50(4): 305–314, doi: 10.1007/s10735-019-09827-x, indexed in Pubmed: 31028566.
37. Chen W, Li X, Guo S, et al. Tanshinone IIA harmonizes the crosstalk of autophagy and polarization in macrophages via miR-375/KLF4 pathway to attenuate atherosclerosis. Int Immunopharmacol. 2019; 70: 486–497, doi: 10.1016/j.intimp.2019.02.054, indexed in Pubmed: 30870679.